AGU PUBLICATIONS

Global Biogeochemical Cycles

RESEARCH ARTICLE
10.1002/2014GB005044

Key Points:
- We estimated CH_4 and DIC production mechanisms and CH_4 transport and oxidation
- CH_4 and DIC pore water concentrations were spatially variable in drainages
- Important temporal and watershed-scale effects influenced methanogenic mechanism

Supporting Information:
- Texts A1–A3, Figures A1 and A2, and Tables A1–A6

Correspondence to:
H. M. Throckmorton,
hthrockmorton@lanl.gov

Citation:
Throckmorton, H. M., et al. (2015), Pathways and transformations of dissolved methane and dissolved inorganic carbon in Arctic tundra watersheds: Evidence from analysis of stable isotopes, *Global Biogeochem. Cycles*, *29*, 1893–1910, doi:10.1002/2014GB005044.

Received 24 NOV 2014
Accepted 2 SEP 2015
Accepted article online 9 SEP 2015
Published online 8 NOV 2015

Pathways and transformations of dissolved methane and dissolved inorganic carbon in Arctic tundra watersheds: Evidence from analysis of stable isotopes

Heather M. Throckmorton[1], Jeffrey M. Heikoop[1], Brent D. Newman[1], Garrett L. Altmann[1], Mark S. Conrad[2], Jordan D. Muss[1], George B. Perkins[1], Lydia J. Smith[2], Margaret S. Torn[2], Stan D. Wullschleger[3], and Cathy J. Wilson[1]

[1]Los Alamos National Laboratory, Earth and Environmental Sciences Division, Los Alamos, New Mexico, USA, [2]Lawrence Berkeley National Laboratory, Earth Sciences Division, Berkeley, California, USA, [3]Oak Ridge National Laboratory, Environmental Sciences Division, Oak Ridge, Tennessee, USA

Abstract Arctic soils contain a large pool of terrestrial C and are of interest due to their potential for releasing significant carbon dioxide (CO_2) and methane (CH_4) to the atmosphere. Due to substantial landscape heterogeneity, predicting ecosystem-scale CH_4 and CO_2 production is challenging. This study assessed dissolved inorganic carbon (DIC = Σ (total) dissolved CO_2) and CH_4 in watershed drainages in Barrow, Alaska as critical convergent zones of regional geochemistry, substrates, and nutrients. In July and September of 2013, surface waters and saturated subsurface pore waters were collected from 17 drainages. Based on simultaneous DIC and CH_4 cycling, we synthesized isotopic and geochemical methods to develop a subsurface CH_4 and DIC balance by estimating mechanisms of CH_4 and DIC production and transport pathways and oxidation of subsurface CH_4. We observed a shift from acetoclastic (July) toward hydrogenotropic (September) methanogenesis at sites located toward the end of major freshwater drainages, adjacent to salty estuarine waters, suggesting an interesting landscape-scale effect on CH_4 production mechanism. The majority of subsurface CH_4 was transported upward by plant-mediated transport and ebullition, predominantly bypassing the potential for CH_4 oxidation. Thus, surprisingly, CH_4 oxidation only consumed approximately 2.51 ± 0.82% (July) and 0.79 ± 0.79% (September) of CH_4 produced at the frost table, contributing to <0.1% of DIC production. DIC was primarily produced from respiration, with iron and organic matter serving as likely e- acceptors. This work highlights the importance of spatial and temporal variability of CH_4 production at the watershed scale and suggests broad scale investigations are required to build better regional or pan-Arctic representations of CH_4 and CO_2 production.

1. Introduction

Arctic soils contain large C stocks and may be an important source of atmospheric methane (CH_4) and carbon dioxide (CO_2) over the next century due to a rapidly changing climate, degrading permafrost, and redistribution of water across high latitude landscapes [*IPCC*, 2007; *Hinzman et al*., 2005; *Schuur et al*., 2008]. CH_4 and CO_2 productions are influenced by localized microtopographic controls on the water table and available terminal electron acceptors (TEAs) [*Lipson et al*., 2012] and may be affected by combined effects of moisture, season [*Rhew et al*., 2007], vegetation height, active layer depth [*von Fischer and Hedin*, 2007], soil pore size, organic matter chemistry and quantity, temperature [*Roy Chowdhury et al*., 2015], and the presence of vascular rooting systems [*Kruger et al*., 2002]. A better understanding of spatial and temporal variability and relative contributions of factors controlling CH_4 and CO_2 production mechanisms and transport pathways is needed [*Bridgham et al*., 2013], in particular to predict future offsets and unknowns in terrestrial C storage in Arctic ecosystems [*Jorgenson et al*., 2001].

Microtopography along the Arctic Coastal Plain in Alaska is heterogeneous, affecting localized concentrations and availability of TEAs, nutrients, and substrates [*Lipson et al*., 2012; *Heikoop et al*., 2015; *Newman et al*., 2015; *Wainwright et al*., 2015], which presumably plays a large role in localized mechanisms and production of CH_4 and DIC. The modern landscape is characterized by a mix of high- and low-centered polygons [*Billings and Peterson*, 1980; *Zona et al*., 2011], hummocky terrain, thermokarst ponds and lakes, and wetlands [*Arp et al*., 2011]. Much of the landscape is also characterized by different-aged drained thaw lake basins (DTLBs), which

form as lakes drain and become vegetated [*Billings and Peterson*, 1980; *Hinkel et al*., 2003; *Bockheim et al*., 2004]. Polygonal ground develops in basins and interbasin areas due to alternating freeze-thaw cycles, creating ice wedges in the permafrost which uplift terrain, forming polygonal-shaped features with low elevation centers surrounded by high rims and low troughs that eventually may subside into high-centered polygons with low surrounding troughs. This landscape heterogeneity presents challenges in ecosystem-scale assessment and predictions of CH_4 and CO_2.

Watershed drainages represent a good indicator and integrative signal of broader landscape geochemistry, substrates, and nutrient availability, and have the potential to be an important source of CH_4 and DIC as saturated environments. Given the importance of biogeochemistry to the cycling of C in Arctic ecosystems, our objectives were to use naturally occurring isotopic and geochemical tracers to assess production and transformation of CH_4 and DIC in saturated drainages in Northern Alaska during July and September of 2013. Our sampling approach in drainages was intended to circumvent effects of microtopography and hydrology on variations in substrate or nutrient availability across the landscape.

During our field campaigns in 2013, sampled drainages ranged from stagnant wetlands to slow moving streams, which are typical for summer months in this region. The majority of lateral runoff typically occurs earlier in the spring season during an abrupt snowmelt period lasting approximately 2 weeks [*Zhang et al*., 2000]. Due to frozen ground impeding internal drainage during spring snowmelt, vertical infiltration is minimal. During the subsequent summer months, active layer thaw depth increases, and with summer rain and active layer ice thaw, soils can become saturated. However, typically during summer months, evaporation exceeds precipitation, resulting in a reduction of wetland extent and disconnection of hydrological systems with minimal surface runoff occurring primarily only after heavy summer rain events [*Mendez et al*., 1998; *Bowling et al*., 2003; *Woo et al*., 2008]. Overland flow largely ceases as drainage networks including channels, lakes, ponds, and wetlands become fragmented [*Mendez et al*., 1998; *Rovansek et al*., 1996; *Bowling et al*., 2003]. Thus, in situ production and vertical transport processes within the depth profile through the thawed active layer typically dominate over lateral transport of CH_4 and DIC in these environments during summer months and at the time of our sampling campaigns.

When lateral transport is minimal, the $\delta^{13}C$ signature of coexisting dissolved CH_4 and DIC and variations in CH_4 and DIC $\delta^{13}C$ values in pore waters with depth, can provide insight into C cycling pathways. Pathways and isotopic fractionations associated with CH_4 and DIC production that provided a basis for our approach are summarized in Figure 1. Characteristically, $\delta^{13}C$ values of dissolved CH_4 and DIC provide information about methanogenic pathways (acetoclastic vs. hydrogenotrophic) (Figure 1, pathways B and C) [*Whiticar*, 1999; *Conrad*, 2002; *Chanton*, 2005]. Isotope mass balance mixing models can be applied to estimate the proportion of DIC derived from (1) respiration and organic matter fermentation, which are nonfractionating (Figure 1, pathway D), relative to (2) DIC from methanogenesis (Figure 1, pathway A) [*Corbett et al*., 2013] in the absence of significant CH_4 oxidation.

DIC production by anaerobic respiration is thermodynamically favorable to, and may inhibit, CH_4 production where TEAs (NO_3^-, SO_4^{2-}, Mn, Fe oxide, and oxidized organic matter) are available and primary methanogenic substrates (acetate and H_2) are limited [*von Fischer and Hedin*, 2007]. CH_4 release to the atmosphere may also be mitigated if subsurface CH_4 diffusing toward the surface becomes oxidized in pore waters [*Whiticar*, 1999; *Kruger et al*., 2002]. The mechanism of upward transport of CH_4 may occur via three mechanisms including (i) plant-mediated transport via either molecular diffusion or bulk flow, (ii) ebullition, and (iii) diffusion through soil pores and the soil column, herein referred to as "diffusion" [*Schütz et al*., 1991; *Chanton*, 2005]. Plant-mediated transport and ebullition (Figure 1, pathway H) of CH_4 are less susceptible to oxidation relative to diffusion (Figure 1, pathway G) [*Happell et al*., 1994; *Chanton*, 2005], which ultimately influences relative release of CH_4 versus CO_2 to the atmosphere. Mass balance isotopic approaches can approximate plant-mediated transport and ebullition together (Figure 1, pathway H) relative to diffusion (Figure 1, pathway G) [*Corbett et al*., 2013]. CH_4 oxidation in pore waters has implications for CH_4 and CO_2 emissions (Figure 1, pathway E) and can also be estimated using isotopic approaches [*Whiticar*, 1999; *Mahieu et al*., 2008; *Preuss et al*., 2013; *Corbett et al*., 2013].

Our objectives were to assess the dominance of either acetoclastic or hydrogenotrophic methanogenic pathways and to approximate the partitioning of vertical CH_4 transport mechanisms. Further, we aimed to estimate DIC production mechanisms from respiration, methanogenesis, and CH_4 oxidation; and to assess

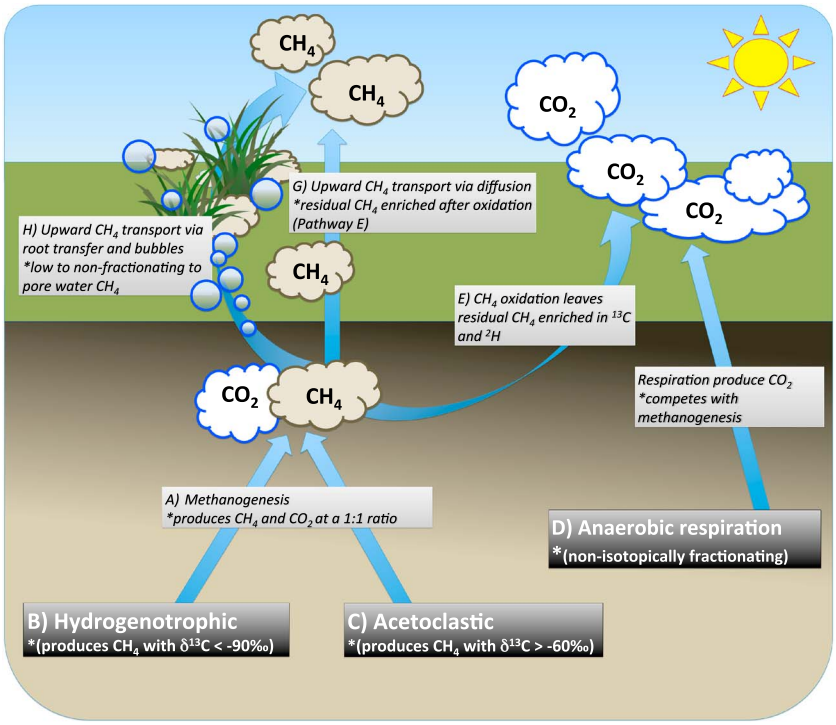

Figure 1. Belowground C cycling pathways and isotopic effects.

pore water geochemistry to infer potential TEAs contributing to anaerobic DIC production. This work was intended to provide insight into spatial (vertical and lateral) and temporal (July vs. September) variability in CH_4 and DIC concentrations and processes across arctic watershed drainages with different geomorphology and properties. Additionally, our methodology may serve as a template that can similarly be applied in other studies in the Arctic or other wetland environments to infer spatial and temporal variability and localized effects influencing CH_4 and DIC processes.

2. Materials and Methods

2.1. Site Description

During July and September of 2013, we collected soil pore waters from 17 drainages in and around the Barrow Environmental Observatory in Barrow, AK, USA. Soils are classified as typic histoturbels (surface organic layers 20–40 cm thick) and aquiturbels (surface organic layers $<$ 20 cm thick), with an organic layer overlying fine, silt-rich lacustrine sediments [*Bockheim and Hinkel*, 2005]. Vegetation in higher elevation areas is dominated by mosses (*Sphagnum*, *Dicranum*, and *Polytrichum* sp.), and vegetation in low elevation saturated areas (including drainage sampling locations; Figure 2) is dominated by a mixture of sedges (*Carex aquatilis* and *Eriophorum* sp.) and mosses (*Drepanocladus* and *Sphagnum* sp.) [*Villarreal et al.*, 2012; *Sloan et al.*, 2014].

Liquid active layer water samples were collected from three depths at each location including (1) surface waters, (2) "shallow" subsurface (7.5–15 cm from surface), which was commonly an organic soil horizon, and (3) the bottom of the active layer ("deep"; maximum depth to the frost table $<$ 64 cm, often a mineral-rich horizon), which varied with depth across sites from July (33.8 ± 1.7 cm) to September (43.3 ± 2.0 cm) (Table A1 of the supporting information). We define the frost table as the upper surface of ice-bonded material and the active layer thaw depth as the depth from the soil or water surface to the upper limit of ice-bonded material [*Owens and Harper*, 1977]. The frost table begins to thaw from the surface in spring and reaches maximum depth in fall just before winter frost, which is consistent with our deeper measurements of the frost table in September than in July for our study. We measured depth to frost table by probing the soft thawed active layer until we detected frozen ground as a dense frozen layer. Sampling locations were stationed along the periphery of internal and external drainages, draining from different-aged drained thaw lake basins (DTLBs); different types of polygonal terrain, ranging from high- to low- centered; and interlake

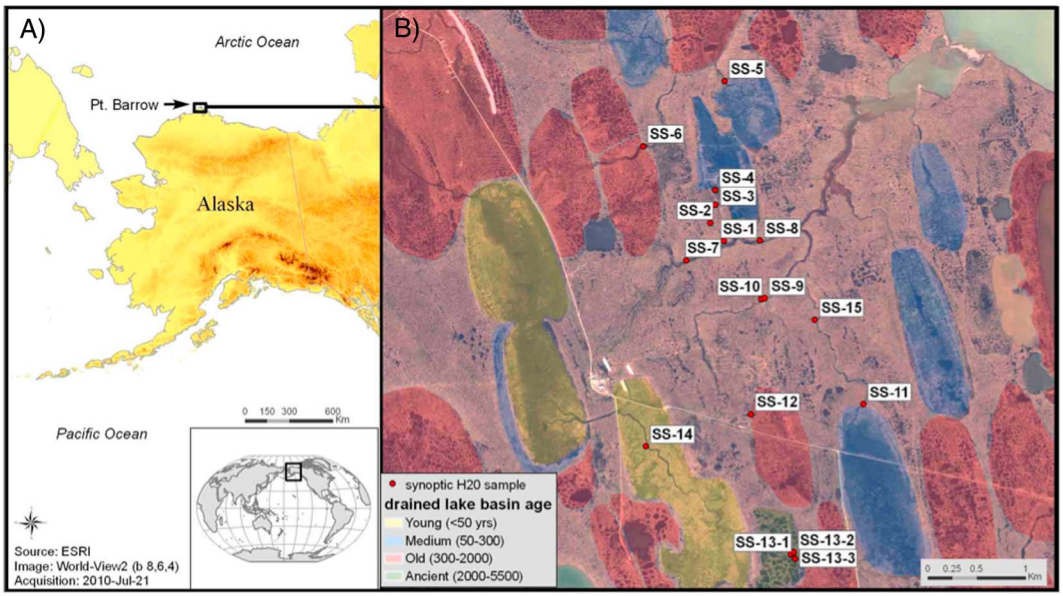

Figure 2. (A) Location of Barrow, Alaska, USA. (B) Location of synoptic water sampling sites at drainages, sampled in July and September, 2013. Colors indicate different-aged drained thaw lake basins (DTLBs, see inset legend for ages).

basin areas (Figure 2 and Table A1; section 2.2). Watersheds were delineated using the Spatial Analyst extension in ArcGIS 10.2 applied to digital elevation models. Verification and some manual postprocessing were necessary due to the low relief surface topography [e.g., *Arp et al.*, 2012]. Watersheds with selected drainages were classified as follows: interlake basins containing polygonal terrain, different-aged DTLBs [young (<50 years), medium-aged (50–300 years), old (300–2000 years), or ancient (2000–5500 years)] [*Hinkel et al.*, 2003], or a combination of watersheds integrating different-aged DTLBs and interlake areas (Table A1; "Watershed" classification). Sampled drainages were further classified by flow activity ("Flow Type") as either stagnant wetlands with no observable flow upon sampling or channels where gentle lateral surficial flow was noted upon sampling (Table A1). In cases where gentle lateral flow was observed in the drainage channel, the periphery of channels where water was extracted always appeared stagnant.

2.2. Surface Water and Soil Pore Water Collection

Surface waters were collected as grab samples from the edges of drainages. For shallow active layer samples, one stainless steel drive point sampler (2.1 cm I.D.) was installed at each sampling location, with pore openings and collection depths ranging from 7.5 to 15 cm below the soil surface. Tubing was installed into the drive point opening (Masterflex platinum-cured silicone), and water was slowly siphoned into 1 L bottles (HDPE, Nalgene) using a hand-pump vacuum. For the collection of deeper samples, 14–20 macro-rhizon [*Seeberg-Elverfeldt et al.*, 2005] samplers were installed in an array (30 cm apart) down to the frost table. Multiple macro-rhizons were used to obtain sufficient water volume for chemical analyses; these were more effective than drive points for collecting water from the deeper active layer. Depth to frost table was measured at each rhizon location and averaged within a site. The frost table depth (and collection depth for "deep" samples) varied by location and time (Table A1). Results for deep soil pore water provide insight into geochemistry and isotopic signatures at the top of the frost table, rather than a specific depth from the surface. For time-sensitive or oxidation-sensitive analytes [Fe^{2+}, dissolved oxygen (DO), dissolved CH_4, and DIC], 2–3 syringes (60 mL) were removed as soon as enough water was available for analyses (within 30 min of sampling), and pore water in syringes was composited prior to analyses. Rhizons and syringes were reinstalled, and after approximately 2 h of sampling, water in the remaining syringes was composited for all other analyses and processed and/or analyzed in the field (section 2.3).

2.3. Field Measurements and Sample Processing

Fe^{2+}, temperature, DO, and pH were measured in the field on unfiltered pore waters immediately after extraction. Fe^{2+} was measured with a (Ferrous) Color Disc Test Kit (Hach, IR-18C), DO with a Hach luminescence DO

meter (HQ30d), and temperature with a thermal meter with internal temperature reference (Thermo Scientific 927007MD). Waters collected for total dissolved Fe (Fe^{Total}) were filtered in the field (0.45 μm, Fisher syringe filters) and acidified for preservation with concentrated nitric acid within 48 h of collection (pH < 2). Samples collected for CH_4 and DIC concentrations and $\delta^{13}C$ isotopes were filtered in the field (0.2 μm, Fisher syringe filters) during injection into pre-evacuated 60 mL glass bottles with blue butyl rubber septa. Samples collected for DOC were filtered in the field (0.45 μm, Fisher syringe filters) and stored in 40 mL glass vials. All other samples collected in the field (i.e., for CH_4, DIC, and DOC concentrations and isotopes, and anions) were stored in coolers over ice packs in 60 mL bottles (HDPE, Nalgene) and transferred into a 4°C cold room within 18 h of collection (Barrow Arctic Research Center, Barrow, AK, USA). Within 2 weeks after collection, samples were transported in coolers on ice packs to the Geochemistry and Geomaterials Research Laboratory (GGRL), Los Alamos National Laboratory (LANL) (Los Alamos, NM, USA), where they were stored at 4°C until analyzed (section 2.4).

2.4. Surface Water and Soil Pore Water Measurements

All laboratory analyses were conducted at the GGRL. Fe^{Total} was measured along with major cations and trace metals by inductively coupled plasma optical emission spectrometry and inductively coupled plasma mass spectrometry utilizing EPA methods 200.7 and 200.8. The Perkin Elmer Optima 2100 DV and Elan 6100 were the specific systems utilized. Ultra high-purity nitric acid (Fisher Trace Metal Grade) was used in sample and calibration preparation prior to sample analysis. Internal standards (Sc, Ge, Bi, and In) were added to both samples and standards to correct for matrix effects which can result in differing sample introduction rates. Some samples were diluted prior to analysis in order to minimize matrix effects as well as allow the analytes of interest to remain within the linear dynamic range of the calibration. Standard Reference Material 1643e Trace Elements in Water was used to check the accuracy of the multi-element calibrations.

Fe^{3+} was calculated as the difference between Fe^{Total} and Fe^{2+} measured in the field. For a few samples with low Fe^{Total} (<1 mg L^{-1}), where $Fe^{2+} > Fe^{Total}$, Fe^{2+} values were adjusted to equal Fe^{Total}. The oxidation state of Fe was calculated as the percentage of $Fe^{2+}/Fe^{Total} * 100\%$ for the reduced portion (Fe^{Reduc}) and $Fe^{3+}/Fe^{Total} * 100\%$ for the oxidized portion (Fe^{Oxid}) [*Lipson et al*., 2013]. Inorganic anion samples were analyzed by ion chromatography following United States Environmental Protection Agency method 300 on a Dionex DX-600 system.

Dissolved organic nitrogen (DON) was determined using the alkaline persulfate oxidation method [*Cabrera and Beare*, 1993]. DON in 1 mL of groundwater was oxidized to NO_3^- with 0.5 M potassium sulfate, and NO_3^- concentrations were determined using a single reagent method [*Doane and Horwath*, 2003]. Spectral absorbance was measured at 540 nm and calibrated against NO_3^- standards. For DIC concentrations and $\delta^{13}C$-DIC, approximately 1 mL of groundwater was removed through septa of the glass bottles with a needle and syringe and injected into a helium-purged vial, and the mass of the water was measured. CO_2 was extracted from DIC by acidification with 103% orthophosphoric acid (H_3PO_4) at 50°C. The evolved CO_2 was measured on a GV Instruments Isoprime continuous flow isotope ratio mass spectrometer (GV Instruments, Manchester, UK) coupled to a Multiflow peripheral instrument. $\delta^{13}C$ results are reported relative to V-PDB and calibrated to CO_2 derived from IAEA carbonate standards NBS-18, NBS-19, and LSVEC. The concentrations were determined by using a calibration curve relating mass spectrometer response versus the DIC concentration in a $NaHCO_3$ standard.

CH_4 concentrations were determined by GC-FID using an Agilent GC 6890A with an HP-Plot column 250 μL injection of headspace gas. The headspace CH_4 concentration was determined based on a calibration curve using CH_4 diluted to varying concentrations. Dissolved CH_4 concentrations were determined based on the Henry's law partitioning between dissolved and gaseous CH_4. $\delta^{13}C$ values of CH_4 were measured with a MassLynx Isoprime stable isotope ratio mass spectrometer coupled to a TraceGas peripheral. The injection volume was varied by sample to aim for constant mass spectrometer response and eliminate nonlinearity effects. $\delta^{13}C$-CH_4 values were calibrated from an in-house methane standard (LANL 1258282) which had been calibrated from IAEA standards and independently analyzed. Prior to injection, CH_4 bottles were shaken on a mechanical shaker for ~24 h to equilibrate headspace with water samples.

ε_c was calculated as the difference between $\delta^{13}C$ of total dissolved CH_4 and $\delta^{13}C$ of total DIC on a per sample basis and will be considered in inferring methanogenic pathway [*Whiticar*, 1999]. The apparent fractionation factors for DIC → CH_4 (α) were calculated as follows:

$$\alpha = \frac{\delta^{13}C_{DIC} + 1000}{\delta^{13}C_{CH_4} + 1000} \quad (1)$$

Similarly, α-values have been used to infer methanogenic pathways, where larger α-values are typical of hydrogenotrophic methanogenesis and smaller values are typical of acetoclastic [*Whiticar et al*., 1986; *Whiticar*, 1999; *Conrad*, 2002; *Chanton*, 2005; *Hines et al*., 2008].

2.5. Pathway Estimates

2.5.1. Estimating DIC From Methanogenesis Versus Respiration

A series of isotope mass balance equations were used to estimate (1) the proportion of DIC produced from nonfractionating organic matter respiration and fermentation, relative to (2) DIC produced from methanogenesis, a fractionating process, in pore water samples collected at the frost table, following methods by *Corbett et al*. [2013]. We separately considered pore water samples from shallow depths, which are subject to oxidation. We assumed no DIC was from the dissolution of carbonates in mineral soils based on low pH and based on the fact that carbonates have not been identified in these soils.

We assume that the isotopic composition of CH_4 collected from deeper pore waters at the frost table represents that of newly produced CH_4 with negligible oxidation [following *Popp et al*., 1999; *Hines et al*., 2008]. While in some cases oxygen could potentially be delivered downward from rooted vascular plants to promote CH_4 oxidation at depth [*Corbett et al*., 2013], the fact that frost table samples occurred below the rooting depth and low oxygen levels measured in deep pore waters suggests that aerobic CH_4 oxidation in deep samples at the frost table would likely be insignificant. Additionally, our approach assumes negligible anaerobic oxidation of CH_4 for deep pore water samples, which has recently been shown to occur in peat soils incubated under standard conditions (19°C) [*Gupta et al*., 2013]. However, the occurrence of anaerobic CH_4 oxidation in situ in Arctic tundra is unknown, and potential effects on deep CH_4 ^{13}C, and uncertainty introduced on estimates of deep DIC sources are beyond the scope of this study. For shallow pore waters, we estimated the potential error introduced from CH_4 oxidation to our estimates of shallow subsurface DIC source to be negligible (Text A1).

The theory and application of the applied isotope mass balance approach is described in detail in *Corbett et al*. [2013] and can account for both pathways of methanogenesis (Figure 1, pathways B and C). Briefly, we first determined the $\delta^{13}C$-DIC resulting from methanogenesis using the measured values of $\delta^{13}C$-CH_4 and the $\delta^{13}C$-OM [rearranged from *Corbett et al*., 2013]:

$$\left(\delta^{13}C - DIC_{meth}\right) = \frac{\left(\delta^{13}C - OM\right) - (0.5)\cdot\left(\delta^{13}C - CH_4\right)}{(0.5)} \quad (2)$$

This approach relies on the assumption that equal amounts of CH_4 and DIC are produced during methanogenesis from DOC [*Chanton*, 2005], which is typical for peat and wetland soils [*Conrad*, 1999]. We assume that measured CH_4 $\delta^{13}C$ values in deep and shallow soil pore waters approximate the CH_4 initially produced after methanogenesis ($\delta^{13}C - CH_4$). The isotope mass balance between ($\delta^{13}C - DOC$) and ($\delta^{13}C - CH_4$) allows us to solve for ($\delta^{13}C - CO_{2\,-\,meth}$) in equation (2).

We assumed that DIC produced from respiration and fermentation would have a $\delta^{13}C$ isotopic signature equal to organic matter substrate ($\delta^{13}C$–OM) from which it derived [*Lapham et al*., 1999], which we approximated with the mean of our measured $\delta^{13}C$ DOC isotope signatures in subsurface pore waters. After determining the $\delta^{13}C$-CO_2 from methanogenesis [equation (2)], the fraction of CO_2 from either isotopic fractionating methanogenesis ($fCO_{2\,-\,meth}$) (Figure 1, pathway A) or nonfractionating OM respiration and fermentation ($fCO_{2\,-\,OMdecay}$) (Figure 1, pathway D) was estimated:

$$\left(\delta^{13}C\text{–}CO_2\right) = \left(\delta^{13}C\text{–OM}\right)\cdot\left(fCO_{2-OMdecay}\right) + \left(\delta^{13}C\text{–}CO_{2-meth}\right)\cdot\left(fCO_{2-meth}\right) \quad (3)$$

and

$$fCO_{2-OMdecay} + fCO_{2-meth} = 1 \quad (4)$$

where $\delta^{13}C–CO_2$ is the measured total $\delta^{13}C$ of CO_2 from pore water, $\delta^{13}C–CO_{2-meth}$ is the calculated $\delta^{13}C$ of CO_2 from methanogenesis [equation (2)], and $fCO_{2-OMdecay}$ is the fraction of CO_2 from respiration and fermentation [*Corbett et al*., 2013]. Combining equations (3) and (4) and solving for two unknown variables allowed us to estimate fCO_{2-meth} and $fCO_{2-OMdecay}$ [*Corbett et al*., 2013]. This approach does not account for any possible isotopic fractionation of CH_4 in the rhizosphere from plant-mediated transport. Isotopic fractionation that has been shown to occur during diffusive plant-mediated transport is primarily attributed to fractionation in the plant aerenchyma as CH_4 gas exits the plant to the atmosphere, rather than CH_4 transport into the plant through root uptake in the rhizosphere [*Chanton*, 2005]. Potential rhizosphere fractionation is not well understood; however, if root-based fractionation of CH_4 in the rhizosphere were to occur, our approach would overestimate CH_4 oxidation and underestimate CO_2 produced from nonfractionating pathways [*Corbett et al*., 2013]. We estimated the error introduced by diffusion on fCO_{2-meth} to be negligible (Text A2). An additional possible transport mechanism, advection, is not considered to be significant in subsurface soil pore waters due to the low hydrologic gradients and low permeability soils, but is considered in surface waters in section 3.2.2 with comparisons of stagnant and gently flowing drainages showing no differences for a number of variables tested, suggesting that in situ processes and vertical transport via diffusion are likely dominant over advection or lateral transport effects.

2.5.2. Estimates of Upward Subsurface CH_4 Transport Via Ebullition and Plant-Mediated Transport

The approach in section 2.5.1 estimates the *combined loss* of dissolved CH_4 from drainage systems by (1) ebullition due to low CH_4 solubility and (2) vascular plant transport (Figure 1, pathway H). This approach maintains the assumption that DIC and CH_4 produced from methanogenesis [equation (2)] should occur at an equimolar ratio (1:1) in solution. Any discrepancy in molar ratio of measured CH_4 to calculated DIC produced during methanogenesis is attributed to CH_4 loss via ebullition and vascular plant transport [equation (5)] [*Corbett et al*., 2013], while measured dissolved CH_4 in solution is the fraction of upwardly diffusing CH_4 (Figure 1, pathway G).

$$CH_{4-Trans} = CO_{2-meth} - CH_{4-Measured} \tag{5}$$

where ($CH_{4-Trans}$) is the combined loss of subsurface CH_4 to ebullition and plant transport (molar), (CO_{2-meth}; i.e., = CH_4 production by assuming equimolar production via methanogenesis) is CO_2 produced from methanogenesis [equation (3)] (converted to molarity as the fraction of measured DIC in deep pore waters), and $CH_{4-Measured}$ is measured CH_4 in pore water associated with diffusion. $CH_{4\text{-}Trans}$ and $CH_{4\text{-}Measured}$ were converted to and expressed as percentages of total CH_4 produced. Molar concentrations were converted to percentages for CH_4 and CO_2 ($fCH_{4\text{-}Trans}$, $fCO_{2\text{-}meth}$, and $fCH_{4\text{-}Measured}$). CH_4 transport was estimated separately for deep and shallow subsurface pore waters. Errors introduced from CH_4 oxidation on estimates of CH_4 and DIC from methanogenesis were estimated to be negligible (Text A3).

2.5.3. Estimating CH_4 Oxidation With "Open System Estimates"

We applied an "open system" estimate for CH_4 oxidation occurring throughout the vertical soil profile (Figure 1, pathway E) [*Monson and Hayes*, 1980; *Mahieu et al*., 2008; *Preuss et al*., 2013]. This approach considers isotopic composition of deep pore waters relative to surface waters:

$$f_{ox} = \frac{(\delta_E - \delta_P)}{1000 \cdot (\alpha_{ox} - \alpha_{trans})}, \tag{6}$$

where f_{ox} is the fraction of deep CH_4 oxidized in the soil, δ_E is the $\delta^{13}C$ of surface CH_4, δ_P is the $\delta^{13}C$ of CH_4 in deep pore waters, α_{ox} is the isotope fractionation factor for oxidation, and α_{trans} is an isotopic fractionation factor for CH_4 transport, which occurs during diffusion and is a property of the specific gas and medium [*Chanton*, 2005]. These approaches rely on upward diffusion through pore waters, which is relevant to our sampling locations along the edges of drainages (demonstrated in section 3.2.2). Again, we assumed that the CH_4-$\delta^{13}C$ value of deep pore waters was representative of newly produced CH_4 and that discrepancies between surface water and deep pore water $\delta^{13}C$-CH_4 reflected biological isotopic fractionation associated with oxidation only. This approach relies on no significant shift in mechanisms of methanogenesis from deep to shallow subsurface samples, which would affect the $\delta^{13}C$ of newly produced CH_4, which we determined was appropriate for our study. Under conditions where methanogenic mechanisms do vary with depth, with acetoclastic methanogenesis occurring in shallower horizons (producing isotopically enriched CH_4) and hydrogenotrophic methanogenesis occurring in deeper underlying horizons (producing isotopically depleted CH_4), our approach would overestimate methane oxidation. For our particular study we determined

this assumption is valid based on predominance of acetoclastic methanogenesis in deep samples, with no relationship between deep CH_4 isotopes and CH_4 oxidation estimates within the depth profile (see section 3.2.1) Although α_{trans} may differ for organic and mineral horizons, any variations in this coefficient would have little effect on our results. We applied 1.001 as the α_{trans} coefficient, which is the only value reported for saturated soils and, according to *Preuss et al*. [2013], is a good approximation. Oxidation estimates are more sensitive to variations in the microbial oxidation isotopic factors (α_{ox}) [*Preuss et al*., 2013]. α_{ox} coefficients ranging from 1.003 to 1.049 have been reported [*Reeburgh et al*., 1997; *Templeton et al*., 2006; *Cabral et al*., 2010]. We applied 1.031 as α_{ox} in our estimates, which was reported as a maximum value in water-saturated organic soils in Arctic Siberia [*Preuss et al*., 2013], with conditions similar to our field sites. While we acknowledge this is an approximation, we conservatively assume that this is likely the maximum α_{ox} based on our soils and environmental conditions, and should result in *minimum* approximations of the amount of CH_4 oxidized during diffusion. The fraction of CH_4 oxidization (f_{ox}) between deep and surface water was calculated using isotopic difference [equation (6)], and a molar conversion was applied to estimate the molar fraction (%) that CH_4 oxidation would contribute to DIC production in the vertical soil profile during upward diffusion. Ideally, this estimate would be expressed as a percentage of surface DIC concentrations (i.e., production); however, due to atmospheric interaction with surface water DIC (discussed in sections 3.2.1 and 4.1), we considered shallow subsurface pore water DIC concentrations rather than surface DIC concentrations to approximate the contribution of CH_4 oxidation to DIC production in the soil profile relative to alternative mechanisms.

2.6. Statistical Analyses

General linear models were used to test effects on CH_4, DIC, and DOC concentrations, described throughout section 3. For numeric predictor variables we applied Spearman Permutation Tests (9999 permutations) and one-way Analyses of Variance tests for nominal variables. We applied Pearson Correlation regression analyses to assess linear dependence among variables and to inform linear model analyses. R (v. 2.14.0) was used for all analyses and figures. p-values < 0.05 are considered significant.

3. Results

3.1. Dissolved Oxygen (DO) and Fe

In July and September (2013), surface waters were in near equilibrium with atmospheric oxygen (Table A2; Table A3). There was a decrease in DO with depth, with a corresponding increase of Fe^{2+} and dissolved Fe^{3+} ($<0.45\,\mu M$) (Table A3). Total dissolved Fe (Fe^{Total}) was most concentrated in deeper pore waters in July and September; and the percentage of Fe^{3+} relative to Fe^{Total} was also highest in deep pore waters (Figure 3A). Fe^{Total} concentrations decreased from July to September but were still high, in the range of several hundred milligrams per liter at the frost table (see section 4.5 for discussion). Alternative potential TEAs (NO_3^-, SO_4^{2-}, and dissolved Mn) were either below detection or occurred in low concentrations. There were only four locations with detectable NO_3^- (September only; Sites 1, 13_2, 13_3, and 14), with the highest concentration at $0.87\,mg\,L^{-1}$. SO_4^{2-} was $3.4 \pm 0.9\,mg\,L^{-1}$, with the highest concentration at $63.8\,mg\,L^{-1}$ (September; Site 1). Dissolved Mn concentrations were $0.9 \pm 0.3\,mg\,L^{-1}$, with the highest concentration at $24.6\,mg\,L^{-1}$ (July; Site 1). pH was significantly lower in shallow subsurface pore waters than in deep and surface pore waters in July and September ($p < 0.05$; Table A3).

3.2. CH_4, DIC, and DOC Concentrations and DOC/DON Ratios

CH_4, DIC, and DOC concentrations were significantly related to sampling depth (i.e., surface, shallow, and deep; Table A4; Figures 3B–3D). In July, CH_4 was most concentrated in the shallow subsurface, ranging up to $>1\,mM$. In September, CH_4 concentrations in the shallow subsurface were lower than in July ($p = 0.0051$) and were most concentrated at the frost table relative to shallow and surface waters (Figure 3C). DIC and DOC concentrations significantly increased with depth in July and September (Table A5; Figures 3B and 3D), and DOC was more concentrated in September than in July ($p = 0.0134$) (Table A5; Figure 3B). DOC/DON ratios significantly increased from July to September ($p = 0.0164$; Table A5; Figure 3B).

DIC, CH_4, and DOC were variable across sites, as evidenced by high coefficients of variance (CVs) (Table A5). CVs were 41–64% for DIC, 70–111% for CH_4, and 51–126% for DOC. For CH_4 and DIC, there were no notable

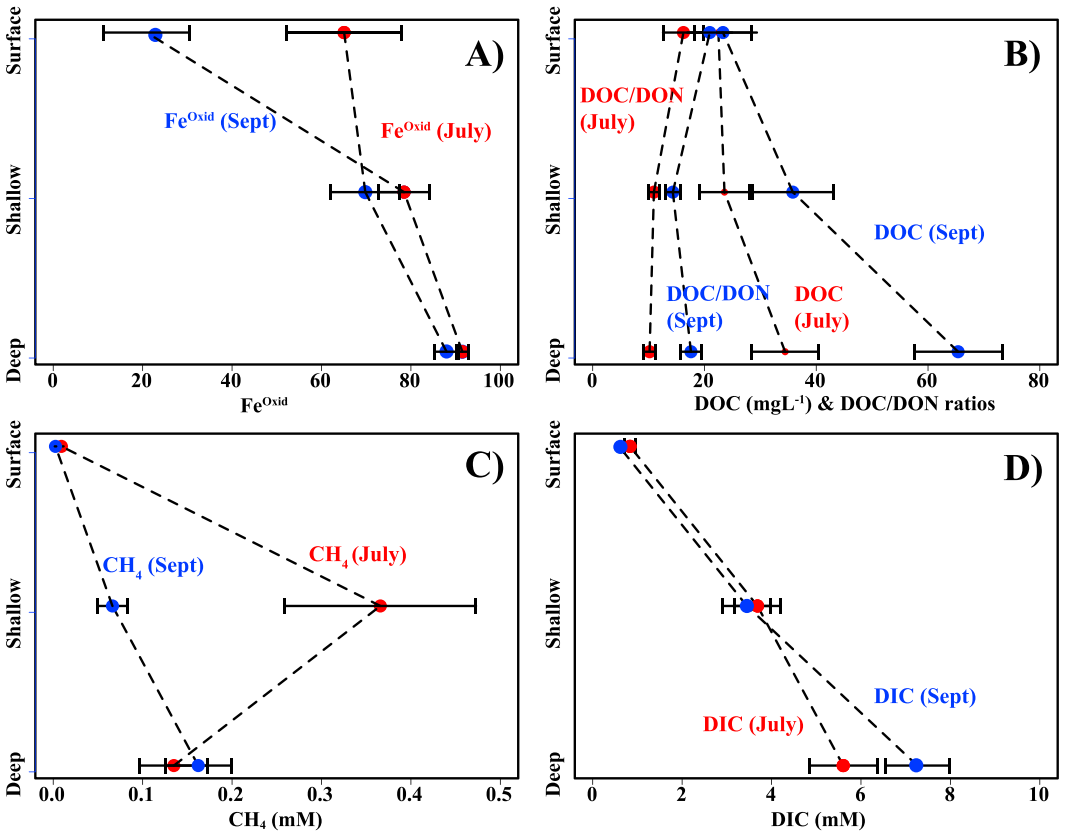

Figure 3. (A) Fe oxidation state (Fe^{Oxid}) expressed as percentage of Fe^{Total} as Fe^{3+} (Fe^{3+}/Fe^{Total}), (B) DOC, (C) CH_4, and (D) DIC concentrations (means and standard errors) for pore water at surface (0 cm), shallow (7.5–15 cm), and deep [bottom of the active layer in July (33.8 ± 1.7 cm) and September (43.3 ± 2.0 cm)].

trends in CVs to suggest more or less variability across sites in surface versus subsurface waters, or during July versus September. DOC was more variable across sites in surface waters, followed by shallow subsurface pore waters, and with the lowest CVs in deep pore waters (Table A5). DOC concentrations significantly differed across sites (Table A4) and were also related to watershed descriptions (Tables 1 and A4). Interlake drainages were relatively concentrated in DOC, along with young, medium, and old DTLBs, while the ancient DTLB and combination watersheds were relatively less concentrated (Figure A1). DOC/DON ratios were 12.5 ± 1.5 in July and 17.6 ± 1.6 in September (means and standard errors for all depths combined). DOC/DON ratios also significantly differed across sites, but these differences were unrelated to watershed properties (Table A4 and Figure A1).

Table 1. The Fraction of Deep Subsurface CO_2 Produced From Respiration ($fCO_{2\text{-}OMdecay}$) and From Methanogenesis ($fCO_{2\text{-}meth}$) as a Percentage of Deep Subsurface CO_2; and Deep Subsurface CH_4 Lost by (i) Plant-Mediated Transport and Ebullition ($CH_{4\text{-}Trans}$) Versus (ii) Diffusion ($CH_{4\text{-}diff}$)[a]

	n	$fCO_{2\text{-}OMdecay}$ (%)			$fCO_{2\text{-}meth}$ (%)			*n*	$CH_{4\text{-}Trans}$			$CH_{4\text{-}diff}$		
July														
Shallow	14	79.4	±	9.1	20.6	±	9.1	14	75.7	±	10.3	24.3	±	10.3
Deep	13	52.8	±	6.1	47.2	±	6.1	14	94.0	±	1.4	6.0	±	1.4
September														
Shallow	15	90.1	±	8.9	9.9	±	8.9	10	94.9	±	2.9	5.1	±	2.9
Deep	15	100.6	±	12.7	−0.6	±	12.7	8	91.2	±	2.9	8.8	±	2.9

[a]Sample size, means, and standard errors shown.

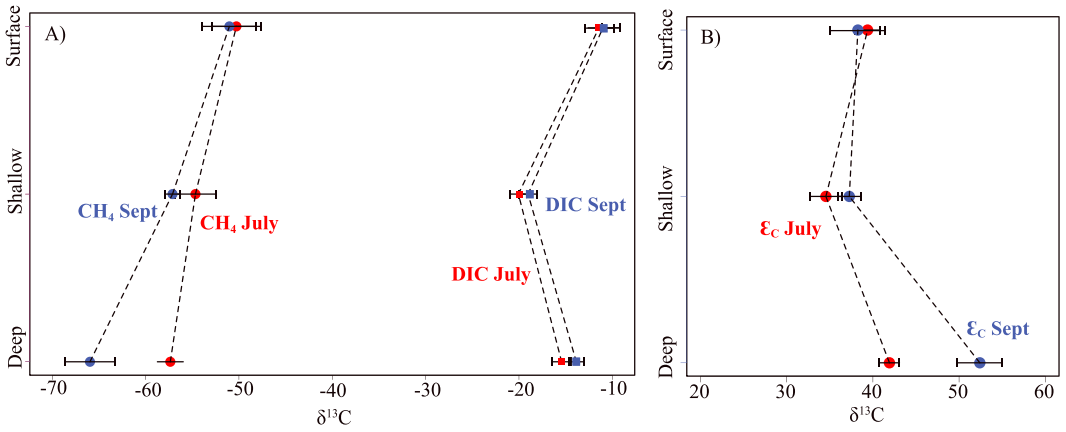

Figure 4. (A) $\delta^{13}C$ plotted for CH_4 and DIC and (B) ε_c values (means and standard errors) for all samples at surface (0 cm), shallow (7.5–15 cm), and deep [bottom of the active layer in July (33.8 ± 1.7 cm) and September (43.3 ± 2.0 cm)].

DIC, CH_4, and DOC positively correlated with Fe^{Total} and Fe^{Oxid}, and negatively correlated with DO; and DIC and CH_4 correlated with Fe^{2+} (Figure A2). DIC and pH were correlated in shallow ($r = 0.46$) and deep ($r = 0.67$) pore waters but not in surface waters ($r = -0.04$). DIC concentrations correlated with Fe^{Total} ($r = 0.66$) and Fe^{Oxid} ($r = 0.56$) in September only ($p < 0.05$). CH_4 concentrations negatively correlated with DO ($p = 0.044$; $r = -0.48$) in shallow subsurface pore waters.

3.2.1. $\delta^{13}C$ of DIC and CH_4

The $\delta^{13}C$ isotope signature of dissolved CH_4 was highest (heaviest) in surface waters and decreased with depth in July and September (Figure 4A), consistent with CH_4 oxidation in shallower samples [*Whiticar*, 1999]. The largest vertical gradient in the $\delta^{13}C$ isotopic profile of CH_4 (surface vs. deep) occurred at Site 5 in July, where the $\delta^{13}C$ of dissolved CH_4 in surface water was enriched by 16.9‰ relative to deep subsurface pore water at the same location (Table A2).

There was also a decrease in the $\delta^{13}C$ of DIC from surface to shallow pore waters, followed by an increase from shallow to deep pore waters (Figure 4A). This change in $\delta^{13}C$ of DIC with depth is likely attributed to changes in the mechanism of DIC formation (i.e., respiration and fermentation vs. methanogenesis; see section 4.5 for further discussion), since we showed the effect of CH_4 oxidation on DIC production and ($\delta^{13}C$-DIC) was negligible (section 2.5.1). The heavy $\delta^{13}C$ of surface DIC may be attributed to dissolution of atmospheric CO_2, which has a $\delta^{13}C$ value of approximately −8.5‰ [*Rubino et al.*, 2013].

$\delta^{13}C$ of deep subsurface CH_4 was significantly depleted in $\delta^{13}C$ in September relative to July ($p = 0.0345$; Figure 4A). In July at the deep subsurface, CH_4 $\delta^{13}C$ ranged from −73‰ (Site 2) to −48‰ (Site 13), and in September, it ranged from −78‰ (Site 9) to −52‰ (Site 13) (Table A2). CH_4 $\delta^{13}C$ values were mostly typical of acetoclastic methanogenesis, with a few exceptions in July and September where deep subsurface CH_4 was relatively depleted in $\delta^{13}C$, potentially reflecting CH_4 from either methanogenic pathway (Table A2; section 4.2). ε_c values ranged from 25 to 65 and generally decreased with depth and increased from July to September at the frost table (Figure 4B). ε_c values were mostly consistent with acetoclastic methanogenesis in deep samples (see section 4.2). ε_c values can also be considered to qualitatively infer trends in oxidation in shallow samples, and within the range of 5–30, they generally indicate strong oxidation (*Whiticar*, 1999). However, due to the fact that ε_c is also influenced by methanogenic mechanism, oxidation cannot be quantified in shallow samples, which vary across sites and over time in our study. ε_c values do however reflect partial methane oxidation in shallow samples consistent with our open system estimates (Table A2). α-values for CH_4-DIC ranged from 1.03 to 1.07, predominantly supporting acetoclastic methanogenesis (Figure 5; see section 4.2 for discussion).

3.2.2. Pathway Estimates

In July, the proportion of DIC from methanogenesis in deep pore waters was 47.2 ± 6.1%, while 52.8 ± 6.1% was from root and microbial respiration and fermentation. In the shallow subsurface in July, DIC sources were 20.6 ± 9.1% and 79.4 ± 9.1% from methanogenesis and respiration with fermentation, respectively. In September, respiration and fermentation produced 100.6 ± 12.7% and 90.1 ± 8.9% of deep and shallow

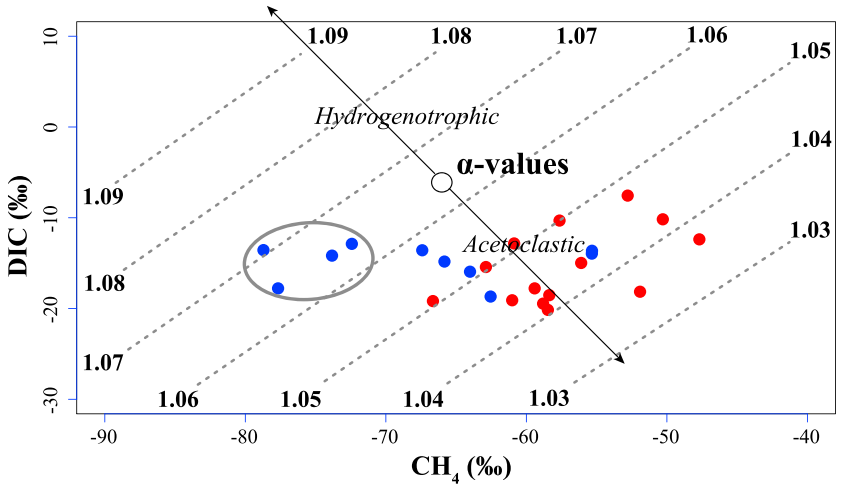

Figure 5. Crossplot of stable C isotope values in deep subsurface pore waters for July (red) and September (blue), 2013. Dotted lines depict α-values. Gray circle indicates September samples that have a hydrogenotrophic fingerprint.

DIC, respectively, while methanogenesis produced $-0.6 \pm 12.7\%$ for deep and $9.9 \pm 8.9\%$ for shallow pore waters (Table 1).

$94.0 \pm 1.4\%$ and $91.2 \pm 2.9\%$ of CH_4 were lost from deep subsurface pore waters via ebullition and plant-mediated transport, while in the shallow subsurface, ebullition and plant-mediated transport removed $75.7 \pm 10.3\%$ in July and $94.9 \pm 2.9\%$ in September (Table 1). The proportion of dissolved CH_4 remaining after loss from ebullition and plant-mediated transport at the frost table was $6.0 \pm 1.4\%$ and $3.4 \pm 5.0\%$ in July and September, respectively, relative to total CH_4 produced. Throughout the soil profile, oxidation consumed

Table 2. The Fraction of (Total) Deep Subsurface CH_4 Consumed by Oxidation During Upward Diffusion From the Frost Table to Surface (%), and Contribution to CO_2 (%) in the Depth Profile[a]

	$CH_{4\text{-}OXID}$		$CO_{2\text{-}OXID}$	
Site No.	July	September	July	September
1	3.5		0.083	
2	0.5		0.004	
3	0.7	1.6	0.007	0.011
4				
5	8.7		0.118	
6	3.9		0.047	
7	5.4		0.043	
8				
9				
10	0.1	0.0	0.001	0.200
11	1.6		0.029	
12	0.6		0.008	
13				
13_2				
13_3				
14	0.0		0.000	
15	2.7		0.025	

CH_4 Oxidation Summary (Mean and Standard Errors Shown)

	July ($n = 11$)			September ($n = 2$)		
$CH_{4\text{-}OXID}$	2.51	±	0.82	0.79	±	0.79
$CO_{2\text{-}OXID}$	0.033	±	0.003	0.071	±	0.037

[a]Missing values are due to insufficient sample availability.

32 ± 5% in July and 55 ± 10% in September of dissolved (diffusing) CH_4, which amounted to only 0.22 ± 0.02% and 0.48 ± 0.25% of total CH_4 produced at the frost table in July and September, respectively.

There may be added uncertainty in estimates of CH_4 oxidation for gently flowing drainages due to effects by lateral transport and mixing; however, there were no significant differences between stagnant and gently flowing drainages in variables including $\delta^{13}C$ DIC, $\delta^{13}C$ CH_4, DIC concentrations, CH_4 concentrations, DO, Fe^{Total}, and CH_4 oxidation, suggesting that in situ processes and vertical transport of CH_4 and DIC likely dominate over lateral transport effects. CH_4 oxidation was variable across sites (Tables 2 and A5), but results suggest that CH_4 oxidation overall had a small effect on total CH_4 and DIC cycling, consuming only 2.51 ± 0.82 in July and 0.79 ± 0.79 in September of total subsurface CH_4 throughout the depth profile from deep to surface and contributing to $<$0.1% to subsurface CO_2 production (Table 1).

4. Discussion

4.1. Dissolved CH_4, DIC, and DOC Concentrations

Due to the high spatial variability observed in aboveground CH_4 and CO_2 efflux from Arctic tundra soils [*Verville et al*., 1998], it is not surprising that we observed such substantial variability in CH_4 and DIC pore water concentrations. Dissolved CH_4 concentrations were even more variable than DIC (Table A4), likely due to CH_4 exsolution from pore waters and ebullition (section 4.3) [*Corbett et al*., 2013]. Saturated soils in mid-late summer are typical for this region [*Hinkel et al*., 2003; *Zona et al*., 2010] and are conducive to the low DO concentrations observed in shallow and deep subsurface pore waters and anaerobic production of CH_4 and CO_2. We observed distinct trends in depth profiles for CH_4 and DIC concentrations and $\delta^{13}C$ isotope signatures, consistent with CH_4 and DIC production and transformations linked to metabolic depletion of DO and alternative TEAs with depth.

While numerous studies have reported on CH_4 efflux [*Torn and Chapin*, 1993; *Christensen et al*., 2004; *Rhew et al*., 2007; *Zona et al*., 2010; *von Fischer et al*., 2010], the literature contains few studies reporting on pore water CH_4 and DIC concentrations in northern latitude drainages. The CH_4 concentrations we measured were similar to pore water concentrations previously reported for northern latitude soils [*Verville et al*., 1998; *Liebner et al*., 2012; *Preuss et al*., 2013]. In July of 2013, the shallow active layer had high CH_4 concentrations, which decreased significantly from July to September. In contrast, DIC concentrations were similar from July to September in the shallow subsurface. These findings may suggest some inhibition of methanogenesis by anaerobic respiration of CO_2 in September, since CH_4 production is less thermodynamically favorable than anaerobic respiration [*von Fischer and Hedin*, 2007].

In both July and September, DIC was most concentrated in deep subsurface pore waters relative to surface and shallow pore waters, presumably produced in situ as deep as the maximum thaw depth. High DO in surface waters suggested near equilibrium with surface waters and the atmosphere. Similarly, the low DIC concentrations in surface waters may also be attributed to atmospheric exchange, which would result in approximately 0.013 mM DIC in equilibrium at 1 atm. DO significantly declined with depth, indicating the need for alternative TEAs for respiration. The increase of DIC from shallow to deep pore waters likely reflected an increased availability of TEAs in mineral soils at the frost table relative to organic-rich soils at the shallow subsurface depths. This hypothesis is supported by our observed increase in dissolved Fe^{3+} with depth, which has been demonstrated as an important e- acceptor in this region [*Lipson et al*., 2010].

DOC concentrations significantly differed across sites and were also related to watershed properties (Table A1). High DOC concentrations were associated with interlake watersheds characterized by polygonal terrain. Polygonal terrain is heterogeneous, and organic matter tends to accumulate in areas of low elevation [e.g., *Zona et al*., 2011], such as drainages where our pore waters were extracted. The trend of decreasing DOC concentrations for DTLBs with increasing age that we observed is consistent with observations that younger basins are generally more productive than older DTLBs [*Zona et al*., 2010]. We also observed significant differences across sites in the DOC/DON ratios, but these differences could not be explained by watershed properties (Figure A1).

4.2. Methanogenic Pathways

Methanogenic pathways were predominantly acetoclastic in July at all locations, and in September, acetoclastic methanogenesis was still the dominant mechanism at 13 of 17 locations, while 4 of 17 locations shifted

toward a predominantly hydrogenotrophic pathway (Sites 3, 9, 10, and 15). We refer the reader to more detailed reviews on background, theory, and applications of applied isotopic approaches [*Whiticar*, 1999; *Chanton*, 2005], but we present several lines of reasoning to support our interpretation. The first line of reasoning was based on typical but distinct $\delta^{13}C$ signatures that occur for CH_4 produced from both mechanisms, with acetoclastic methanogenesis characteristically producing CH_4 $\delta^{13}C$ values $> -60‰$ while hydrogenotrophic is characteristically $< -90‰$, with overlap between $-60‰$ and $-90‰$ for the two mechanisms [*Whiticar*, 1999]. In July and September, deep subsurface pore waters from the majority of locations contained $\delta^{13}C$ CH_4 values $> -60‰$ consistent with acetoclastic methanogenesis, with several locations in the transitional CH_4 $\delta^{13}C$ source field ($< -60‰$ and $> -90‰$) in July and September, potentially reflecting either pathway as being dominant (Table A2). No locations contained CH_4 values $< -90‰$ in deep subsurface pore waters to definitively support a dominant hydrogenotrophic pathway.

However, we also considered the carbon isotope separation factor (ε_c) and the isotope separation factor (α) between coexisting DIC and CH_4 in deep pore waters (section 2.4), which tend to be more informative than the $\delta^{13}C$ of CH_4 alone. In the absence of CH_4 oxidation ε_c values 40–60‰ are characteristic of acetoclastic methanogenesis, while hydrogenotrophic methanogenesis produces ε_c values between 60‰ and 90‰ [*Whiticar*, 1999; *Conrad*, 2002; *Chanton*, 2005]. Using this index, all ε_c values for July deep pore waters were consistent with acetoclastic methanogenesis (Table A2). In September, deep pore waters at Sites 3, 9, 10, and 15 had ε_c values >60‰, consistent with hydrogenotrophic methanogenesis. CH_4-DIC α-values (section 2.4) for these four locations in September ranged from ~1.06 to 1.07, further supporting a hydrogenotrophic pathway [*Whiticar et al*., 1986; *Whiticar*, 1999; *Conrad*, 2002; *Hines et al*., 2008]. Deep $\delta^{13}C$ CH_4 values for these four locations were consistent with a hydrogenotrophic signature in September (ranging between $-60‰$ and $-90‰$). Thus, based on the CH_4 $\delta^{13}C$, ε_c, and α-values of CH_4 in deep pore waters, hydrogenotrophic methanogenesis was the dominant pathway at 4 of 17 drainages (Sites 3, 9, 10, and 15) in September but not in July.

The four locations with predominantly hydrogenotrophic pathways in September (Sites 3, 9, 10, and 15) were draining from interlake or combination watersheds and represented both stagnant and gently flowing drainages, indicating that watershed type and drainage properties could not explain the distinct hydrogenotrophic signature in September at those four locations. However, one interesting trend in the spatial distribution of these four drainages (Sites 3, 9, 10, and 15; Figure 2) is that they are all located outside of DTLBs and are generally located at the edge of the major freshwater drainages right before the transition into salty estuarine waters. The unique spatial distribution of these four locations within the broader drainage network suggests an interesting landscape-scale effect on CH_4 production mechanism, in addition to the temporal effects noted by the differences between July and September.

There were no measured geochemical properties or other factors associated with these sites to explain this distinct shift in methanogenic pathway from July to September at these four locations. Studies suggest that the acetoclastic versus hydrogenotrophic pathway is more likely to occur with increasing pH [*Hines et al*., 2001; *Kotsyurbenko et al*., 2007] and that an acetoclastic pathway is more likely with labile organic substrates with properties such as low C/N ratio, low molecular weight, low aromaticity, low organic oxygen content, and abundant microbial compounds [*Hodgkins et al*., 2014]. Seasonal changes from acetoclastic to hydrogenotrophic methanogenesis as observed in our study have been reported in other studies [*Chasar et al*., 2000] and have been primarily attributed to decline in organic matter quality and depletion of labile C throughout the thaw season [*Hornibrook et al*., 1997; *Hornibrook et al*., 2000; *Chasar et al*., 2000; *Corbett et al*., 2013].

While overall we do report significantly higher DOC/DON ratios in September than in July consistent with the observed trend toward a hydrogenotrophic pathway in September, DOC/DON ratios were not notably higher for those four drainages where a hydrogenotrophic pathway predominantly occurred in September. We acknowledge that DOC/DON ratios provide only a coarse estimate of substrate quality. Additional high-resolution chemical characterization of DOM and its effect on in situ methanogenic pathways across drainage networks and associated watershed drainages may provide further insight into the spatial and temporal variations in methanogenic pathways we observed. Our findings raise additional questions of potential landscape-scale effects on methanogenic pathways that could be addressed in future studies. For example, could the spatial trends (i.e., proximity to the end of freshwater drainages) where acetoclastic methanogenesis

dominated in September be attributed to different substrate chemistries as an outcome of modern transport or erosional processes? Such mechanistic landscape-scale questions could be addressed by measuring the age of organic matter at the frost table across these different drainages, in combination with high-resolution organic matter characterization, to understand whether transport of modern DOC or erosion exposing old DOC may be influencing methanogenic pathways.

Our observations that acetoclastic methanogenesis was a dominant pathway over hydrogenotrophic in this ecosystem in the majority of drainages sampled was somewhat unexpected. Although acetoclastic methanogenesis accounts for approximately 2/3 of CH_4 production from natural systems globally [*Oremland*, 1988], recent metagenomic studies have noted the absence of common acetoclastic microorganisms and abundance of nonacetoclastic microbes in Arctic soils [*Rooney-Varga et al*., 2007]. Additionally, acetate has been shown to accumulate in Arctic soils [*Hines et al*., 2001; *Duddleston et al*., 2002], leading to the belief that temperature may largely influence methanogenesis pathways by inhibiting acetoclastic methanogens [*Rooney-Varga et al*., 2007].

Recent reviews acknowledge that mechanisms of CH_4 production in Arctic soils are not well established and may be spatially variable [*Bridgham et al*., 2013; *Jansson and Tas*, 2014]. The mechanism of methanogenesis (acetoclastic vs. hydrogenotrophic) has been linked to vegetation distribution—specifically the presence or absence of vascular plants, organic matter chemistry, and microbial community structure [*Hines et al*., 2008; *Hodgkins et al*., 2014; *McCalley et al*., 2014]. Consequently, localized or regional shifts in plant or microbial communities have the potential to alter methanogenic pathways as a consequence of warming climate, changing hydrologic regimes, and permafrost thaw in Arctic ecosystems [*McCalley et al*., 2014].

In Barrow, Alaska, localized plant distribution is influenced by microtopography and water table height, with mosses dominating much of the high elevation landscape and a mix of mosses and vascular sedges in low elevation hollows and drainages. Our sampling locations stationed at drainages were relatively saturated and locally dominated by *Carex*, which is suggested to promote an acetoclastic pathway [*Hines et al*., 2008] consistent with our findings. Nonetheless, our results supporting acetoclastic methanogenesis as the dominant pathway may be specific to saturated drainage environments and the presence of vascular plants rather than a region-wide phenomenon along the Arctic Coastal Plain. We suggest more field-based studies are needed with attention to localized effects of microtopography, plant and microbial communities, and organic matter chemistry.

4.3. Methane Transport

Our results are consistent with previous reports that substantial flux of subsurface CH_4 is transported from wetlands to the atmosphere via bubbles and plant roots [*Corbett et al*., 2013]. We estimated that 75.7 ± 10.3% (July) and 94.9 ± 2.9% (September) of shallow subsurface CH_4 were lost due to the combined upward transport of ebullition and plant-mediated transport, while 94.0 ± 1.4% in July and 97 ± 5% in September of deep CH_4 were lost (Table 1; section 2.5.2). Dissolved CH_4 only amounted to 24.3 ± 10.3% in July and 5.1 ± 2.9% in September of subsurface CH_4 produced in the shallow subsurface, and 6.0 ± 1.4% in July and 3.4 ± 5.0% in September of subsurface CH_4 produced at the frost table. These estimates were similar to a study in Northern Minnesota wetlands that reported a loss of 85–100% of subsurface CH_4 due to ebullition and plant-mediated transport [*Corbett et al*., 2013]. These more "direct" transport pathways play a critical role in atmospheric CH_4 and CO_2 flux, since they essentially bypass or minimize the potential for subsurface microbial oxidation. The relative proportion of CH_4 transported via ebullition, plant roots, and diffusion through soil pores depends on a combination of factors such as organic loadings, temperature (including seasonal variations), and plant density and species [*Chanton*, 2005]. Thus, CH_4 transport and oxidation is likely spatially variable with localized variations in factors such as microtopography or plant/microbial communities.

4.4. Methane Oxidation

CH_4 oxidation is the main mitigating process for subsurface CH_4 flux to the atmosphere. We estimated a minimum of 2.5 ± 0.8% in July and 0.79 ± 0.79% in September of deep subsurface CH_4 was oxidized during upward diffusion in pore waters (Table 2 and Figure 6, pathway E). Although CH_4 oxidation overall consumed only a minor portion of subsurface CH_4, there was high variability in CH_4 oxidation across our sampling locations. At one location (Site 5) in September, CH_4 oxidation consumed approximately 8.7% of CH_4

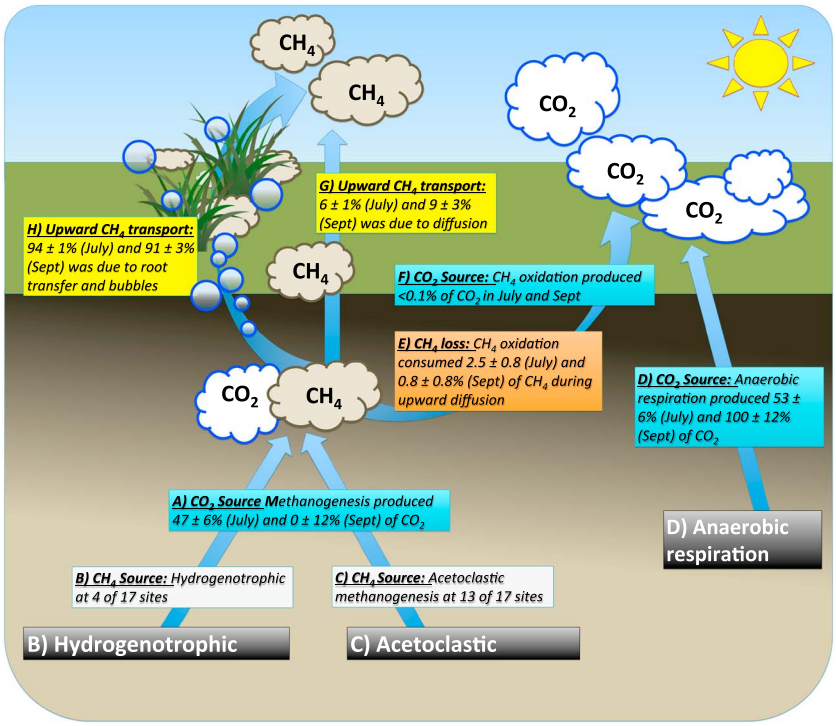

Figure 6. Belowground CH_4 and CO_2 pathway partitioning.

produced at the frost table (Table 2). CH_4 oxidation may be limited by available substrate (i.e., CH_4) [*Lofton et al.*, 2014]; thus, the loss of dissolved CH_4 via ebullition and plant-mediated transport may largely influence CH_4 oxidation, which may also be spatially variable in this region and affected by microtopography and localized plant communities [*Bubier et al.*, 1995; *Whalen et al.*, 1990].

4.5. DIC Production

Organic matter decomposition accounted for the majority of DIC produced (based on estimates in the shallow and deep subsurface pore waters; section 2.5.1) and in September accounted for nearly 100% of DIC (Table 1), with methanogenesis representing the majority of the remaining DIC source. The contribution of CH_4 oxidation to DIC production in the vertical profile was small (<0.1%; section 4.4) relative to respiration and anaerobic fermentation (CO_2) versus methanogenesis (section 3.2.2). The lack of calcite in the soils and low Ca and Mg content of the pore waters indicates that calcite dissolution was also likely not a significant source of DIC [*Chasar et al.*, 2000].

Considering the low DO concentrations, anaerobic respiration via alternative TEAs was more likely to occur than aerobic respiration in subsurface pore waters. Fe oxide and oxidized organic matter (e.g., quinones) have been established as important TEAs in Arctic environments under anaerobic conditions [*Lipson et al.*, 2010]. The unusually high dissolved Fe^{3+} concentrations of our locations were not typical or energetically favorable under corresponding measured pH and Eh [*Brookins*, 1988]; rather, the relatively more abundant Fe phase should have been Fe^{2+}. Similarly high dissolved Fe^{3+} values were previously reported in this region [*Lipson et al.*, 2010] and were attributed to microbial chelation of Fe^{3+} via organic chelating agents such as siderophores [*Lipson et al.*, 2012]. The abundance of Fe^{3+} and DOC, along with correlations among DIC, Fe^{3+}, and DOC, supports the hypothesis that Fe^{3+} and oxidized organic matter are likely important TEAs in this region [*Lipson et al.*, 2010, 2012, 2013; *Keller and Takagi*, 2013].

Alternative potential TEAs (NO_3^-, SO_4^{2-}, and dissolved Mn) were either undetectable or occurred in negligible concentrations and were unrelated to DIC concentrations, suggesting little to no importance of their role in anaerobic respiration. Fe^{Oxid} was significantly related to DIC concentrations in September only, in deep subsurface pore waters ($p < 2e^{-16}$). This correlation, along with the increased Fe^{3+} with depth, supports paired cycling of Fe with anaerobic respiration and CO_2 production. The increasing Fe^{3+} from July to

September supports seasonal cycling of Fe in these systems from reduced to oxidized forms throughout the thaw season, as proposed by *Lipson et al.* [2010].

Anaerobic respiration via reduction of Fe^{3+} and humic substances is thermodynamically favorable over methanogenesis and has the potential to competitively inhibit CH_4 production where substrates such as acetate or molecular hydrogen are limited [*Cervantes et al.*, 2000; *Teh et al.*, 2008; *Klüpfel et al.*, 2014; *Miller et al.*, 2015]. The proportion of subsurface DIC from methanogenesis decreased from July to September, in particular in the deep subsurface (Table 1). There was not a corresponding increase of Fe^{Total} from July to September to inhibit methanogenesis. Additionally, a negative correlation between CH_4 concentrations and any Fe species or Fe^{Oxid} was not observed, which would be expected if methanogenesis were inhibited by Fe^{3+} reduction. Our findings lead to two possible explanations: the first is that TEAs other than Fe may have been acting later in the thaw season to stimulate respiration and inhibit methanogenesis. NO_3^-, SO_4^{2-}, and dissolved Mn were in low concentration, suggesting a possible role from quinones, which we did not measure. The second possible explanation is that organic substrates may be limiting in September, consistent with our hypothesis explaining the shift in methanogenic pathway that occurred from July to September toward increasingly hydrogenotrophic (section 4.2). From July to September, DOC concentrations actually increased while the quality decreased (based on DOC/DON ratio), suggesting that if organic substrate were limiting in September, it would likely be attributed to a decline in organic matter quality and increased recalcitrance from July to September rather than quantity. Both possibilities suggest seasonal change in organic matter quality likely plays an important role in metabolic pathways, as a TEA and/or e-rich substrate.

4.6. Summary

Local drainage channels as examined in this study are critical convergent zones of regional nutrients from watersheds. We applied several approaches to estimate C production and partitioning of transport pathways in Arctic Coastal Plain drainages in northern Alaska. Interestingly, due to the fact that such a large majority of subsurface CH_4 was transported upward via plant-mediated transport and ebullition, oxidation of dissolved CH_4 in pore waters played a very minor role in the subsurface C balance. Another interesting finding of our study was the observed landscape-scale effect on methanogenic pathways, whereby a shift from acetoclastic (July) toward hydrogenotropic (September) methanogenesis occurred at sites located toward the end of major freshwater drainages, adjacent to salty estuarine waters. Substantial spatial and temporal variability in CH_4 and DIC concentrations and metabolic processes across the watershed scale highlights future research opportunities. Further work examining localized effects of microtopography, plant distribution, and organic matter chemistry on CH_4 and CO_2 mechanisms and partitioning is needed. Our results do not imply flux to the atmosphere or production rates but rather provide mechanistic insight into CH_4 and CO_2 production and transport pathways. Studies pairing dissolved C partitioning estimates with aboveground fluxes would be useful for relating mechanisms of production and transformation to atmospheric flux and informing regional C models in the Arctic. Additionally, further work assessing mechanistic questions with high-resolution chemical characterization of substrates across the drainage network in combination with determining the age of organic substrates could help to inform whether transport of new DOC or thermokarst and erosion exposing old DOC may be influencing methanogenic pathways. The latter may be especially important to evaluate as thawing permafrost may drive a dramatic increase in rim and channel bank collapse, as well as lake edge erosion, as climate warms.

Acknowledgments

The data for this paper are available as auxiliary materials and in *Throckmorton et al.* [2015]. The Next-Generation Ecosystem Experiments (NGEE Arctic) project is supported by the Office of Biological and Environmental Research in the DOE Office of Science. Logistical support is provided by UMIAQ, LLC. The authors wish to thank Marvin Gard, Lily Cohen, and Michael Hudak for their support and assistance in fieldwork and preparation, and Emily Kluk, Mike Rearick, and Zackary Vance for their assistance in sample analyses and laboratory management. This work has been authored by an employee of Los Alamos National Security, LLC, operator of the Los Alamos National Laboratory under contract DE-AC52-06NA25396 with the U.S. Department of Energy. The publisher, by accepting this work for publication, acknowledges that the United States Government retains a nonexclusive, paid-up, irrevocable, worldwide license to publish or reproduce this work or allow others to do so for the United States Government purposes.

References

Arp, C. D., B. M. Jones, F. E. Urban, and G. Grosse (2011), Hydrogeomorphic processes of thermokarst lakes with grounded-ice and floating-ice regimes on the Arctic coastal plain, Alaska, *Hydrol. Processes*, *25*(15), 2422–2438.

Arp, C. D., B. M. Jones, Z. Lu, and M. S. Whitman (2012), Shifting balance of thermokarst lake ice regimes across the Arctic Coastal Plain of northern Alaska, *Geophys. Res. Lett.*, *39*, L16503, doi:10.1029/2012GL052518.

Billings, W. D., and K. M. Peterson (1980), Vegetational change and ice-wedge polygons through the thaw-lake cycle in Arctic Alaska, *Arct. Alp. Res.*, *12*(4), 413–432.

Bockheim, J. G., and K. M. Hinkel (2005), Characteristics and significance of the transition zone in drained thaw-lake basins of the Arctic Coastal Plain, Alaska, *Arctic*, *58*(4), 406–417.

Bockheim, J. G., K. M. Hinkel, W. R. Eisner, and X. Y. Dai (2004), Carbon pools and accumulation rates in an age-series of soils in drained thaw-lake basins, Arctic Alaska, *Soil Sci. Soc. Am. J.*, *68*(2), 697–704.

Bowling, L. C., D. L. Kane, R. E. Gieck, L. D. Hinzman, and D. P. Lettenmaier (2003), The role of surface storage in a low-gradient Arctic watershed, *Water. Resour. Res.*, *39*(4), 1087, doi:10.1029/2002WR001466.

Bridgham, S. D., H. Cadillo-Quiroz, J. K. Keller, and Q. L. Zhuang (2013), Methane emissions from wetlands: Biogeochemical, microbial, and modeling perspectives from local to global scales, *Global Change Biol.*, *19*(5), 1325–1346.

Brookins, D. G. (1988), *Eh-pH Diagrams for Geochemistry*, Springer, New York.
Bubier, J. L., T. R. Moore, L. Bellisario, N. T. Comer, and P. M. Crill (1995), Ecological controls on methane emissions from a northern peatland complex in the zone of discontinuous permafrost, Manitoba, Canada, *Global Biogeochem. Cyles*, *9*(4), 455–470.
Cabral, A. R., M. A. Capanema, J. Gebert, J. F. Moreira, and L. B. Jugnia (2010), Quantifying microbial methane oxidation efficiencies in two experimental landfill biocovers using stable isotopes, *Water Air Soil Pollut.*, *209*(1–4), 157–172.
Cabrera, M. L., and M. H. Beare (1993), Alkaline persulfate oxidation for determining total nitrogen in microbial biomass extracts, *Soil Sci. Soc. Am. J.*, *57*(4), 1007–1012.
Cervantes, F. J., S. van der Velde, G. Lettinga, and J. A. Field (2000), Competition between methanogenesis and quinone respiration for ecologically important substrates in anaerobic consortia, *Fems Microbiol. Ecol.*, *34*(2), 161–171.
Chanton, J. P. (2005), The effect of gas transport on the isotope signature of methane in wetlands, *Org. Geochem.*, *36*(5), 753–768.
Chasar, L. S., J. P. Chanton, P. H. Glaser, and D. I. Siegel (2000), Methane concentration and stable isotope distribution as evidence of rhizospheric processes: Comparison of a fen and bog in the Glacial Lake Agassiz Peatland complex, *Ann. Bot. London*, *86*(3), 655–663.
Christensen, T. R., T. R. Johansson, H. J. Akerman, M. Mastepanov, N. Malmer, T. Friborg, P. Crill, and B. H. Svensson (2004), Thawing sub-arctic permafrost: Effects on vegetation and methane emissions, *Geophys. Res. Lett.*, *31*, L04501, doi:10.1029/2003GL018680.
Conrad, R. (1999), Contribution of hydrogen to methane production and control of hydrogen concentrations in methanogenic soils and sediments, *Fems Microbiol. Ecol.*, *28*(3), 193–202.
Conrad, R. (2002), Control of microbial methane production in wetland rice fields, *Nutr. Cycling Agroecosyst.*, *64*(1–2), 59–69.
Corbett, J. E., M. M. Tfaily, D. J. Burdige, W. T. Cooper, P. H. Glaser, and J. P. Chanton (2013), Partitioning pathways of CO_2 production in peatlands with stable carbon isotopes, *Biogeochemistry*, *114*(1–3), 327–340.
Doane, T. A., and W. R. Horwath (2003), Spectrophotometric determination of nitrate with a single reagent, *Anal. Lett.*, *36*(12), 2713–2722.
Duddleston, K. N., M. A. Kinney, R. P. Kiene, and M. E. Hines (2002), Anaerobic microbial biogeochemistry in a northern bog: Acetate as a dominant metabolic end product, *Global Biogeochem. Cycles*, *16*(4), doi:10.1029/2001GB001402.
Gupta, V., K. A. Smemo, J. B. Yavitt, D. Fowle, B. Branfireun, and N. Basiliko (2013), Stable isotopes reveal widespreadh anaerobic methane oxidation across latitude and peatland type, American Chemical Society, *Environ. Sci. Technol.*, *47*, 8273–8279.
Happell, J. D., J. P. Chanton, and W. S. Showers (1994), The influence of methane oxidation on the stable isotopic composition of methane emitted from Florida Swamp Forests, *Geochim. Cosmochim. Acta*, *58*(20), 4377–4388.
Heikoop, J. M., et al. (2015), Isotopic identification of soil and permafrost nitrate sources in an Arctic tundra ecosystem, *J. Geophys. Res. Biogeosci.*, *120*, 1000–1017, doi:10.1002/2014JG002883.
Hines, M. E., K. N. Duddleston, and R. P. Kiene (2001), Carbon flow to acetate and C-1 compounds in northern wetlands, *Geophys. Res. Lett.*, *28*(22), 4251–4254, doi:10.1029/2001GL012901.
Hines, M. E., K. N. Duddleston, J. N. Rooney-Varga, D. Fields, and J. P. Chanton (2008), Uncoupling of acetate degradation from methane formation in Alaskan wetlands: Connections to vegetation distribution, *Global Biogeochem. Cycles*, *22*, GB2017, doi:10.1029/2006GB002903.
Hinkel, K. M., W. R. Eisner, J. G. Bockheim, F. E. Nelson, K. M. Peterson, and X. Y. Dai (2003), Spatial extent, age, and carbon stocks in drained thaw lake basins on the Barrow Peninsula, Alaska, *Arct. Antarct. Alp. Res.*, *35*(3), 291–300.
Hinzman, L. D., et al. (2005), Evidence and implications of recent climate change in northern Alaska and other arctic regions, *Clim. Change*, *72*(3), 251–298.
Hodgkins, S. B., M. M. Tfaily, C. K. McCalley, T. A. Logan, P. M. Crill, S. R. Saleska, V. I. Rich, and J. P. Chanton (2014), Changes in peat chemistry associated with permafrost thaw increase greenhouse gas production, *Proc. Natl. Acad. Sci. U.S.A.*, *111*(16), 5819–5824.
Hornibrook, E. R. C., F. J. Longstaffe, and W. S. Fyfe (1997), Spatial distribution of microbial methane production pathways in temperate zone wetland soils: Stable carbon and hydrogen isotope evidence, *Geochim. Cosmochim. Acta*, *61*(4), 745–753.
Hornibrook, E. R. C., F. J. Longstaffe, and W. S. Fyfe (2000), Evolution of stable carbon isotope compositions for methane and carbon dioxide in freshwater wetlands and other anaerobic environments, *Geochim. Cosmochim. Acta*, *64*(6), 1013–1027.
IPCC (2007), *Climate Change 2007: The Physical Science Basis. Contribution of Working Group I to the Fourth Assessment Report of the Intergovernmental Panel on Climate Change*, edited by S. Solomon et al., Cambridge Univ. Press, Cambridge, U. K., and New York.
Jansson, J. K., and N. Tas (2014), The microbial ecology of permafrost, *Nat. Rev. Microbiol.*, *12*(6), 414–425.
Jorgenson, M. T., C. H. Racine, J. C. Walters, and T. E. Osterkamp (2001), Permafrost degradation and ecological changes associated with a warming climate in central Alaska, *Clim. Change*, *48*(4), 551–579.
Keller, J. K., and K. K. Takagi (2013), Solid-phase organic matter reduction regulates anaerobic decomposition in bog soil, *Ecosphere*, *4*(5).
Klüpfel, L., A. Piepenbrock, A. Kappler, and M. Sander (2014), Humic substances as fully regenerable electron acceptors in recurrently anoxic environments, *Nat. Geosci.*, *7*(3), 195–200.
Kotsyurbenko, O. R., M. W. Friedrich, M. V. Simankova, A. N. Nozhevnikova, P. N. Golyshin, K. N. Timmis, and R. Conrad (2007), Shift from acetoclastic to H-2-dependent methanogenes is in a West Siberian peat bog at low pH values and isolation of an acidophilic *Methanobactetium* strain, *Appl. Environ. Microbiol.*, *73*(7), 2344–2348.
Kruger, M., G. Eller, R. Conrad, and P. Frenzel (2002), Seasonal variation in pathways of CH_4 production and in CH_4 oxidation in rice fields determined by stable carbon isotopes and specific inhibitors, *Global Change Biol.*, *8*(3), 265–280.
Lapham, L., L. Proctor, and J. Chanton (1999), Using respiration rates and stable carbon isotopes to monitor the biodegradation of orimulsion by marine benthic bacteria, *Environ. Sci. Technol.*, *33*(12), 2035–2039.
Liebner, S., S. P. Schwarzenbach, and J. Zeyer (2012), Methane emissions from an alpine fen in central Switzerland, *Biogeochemistry*, *109*(1–3), 287–299.
Lipson, D. A., M. Jha, T. K. Raab, and W. C. Oechel (2010), Reduction of iron (III) and humic substances plays a major role in anaerobic respiration in an Arctic peat soil, *J. Geophys. Res.*, *115*, G00I06, doi:10.1029/2009JG001147.
Lipson, D. A., D. Zona, T. K. Raab, F. Bozzolo, M. Mauritz, and W. C. Oechel (2012), Water-table height and microtopography control biogeochemical cycling in an Arctic coastal tundra ecosystem, *Biogeosciences*, *9*(1), 577–591.
Lipson, D. A., T. K. Raab, D. Goria, and J. Zlamal (2013), The contribution of Fe(III) and humic acid reduction to ecosystem respiration in drained thaw lake basins of the Arctic Coastal Plain, *Global Biogeochem. Cycles*, *27*, 399–409, doi:10.1002/gbc.20038.
Lofton, D. D., S. C. Whalen, and A. E. Hershey (2014), Effect of temperature on methane dynamics and evaluation of methane oxidation kinetics in shallow Arctic Alaskan lakes, *Hydrobiologia*, *721*(1), 209–222.
Mahieu, K., A. De Visscher, P. A. Vanrolleghem, and O. Van Cleemput (2008), Modelling of stable isotope fractionation by methane oxidation and diffusion in landfill cover soils, *Waste Manage.*, *28*(9), 1535–1542.
McCalley, C. K., et al. (2014), Methane dynamics regulated by microbial community response to permafrost thaw, *Nature*, doi:10.1038/nature13798.
Mendez, J., L. D. Hinzman, and D. L. Kane (1998), Evapotranspiration from a wetland complex on the Arctic coastal plain of Alaska, *Nord. Hydrol.*, *29*(4–5), 303–330.

Miller, K. E., C. T. Lai, E. S. Friedman, L. T. Angenent, and D. A. Lipson (2015), Methane suppression by iron and humic acids in soils of the Arctic Coastal Plain, *Soil Biol. Biochem.*, *83*, 176–183.

Monson, K. D., and J. M. Hayes (1980), Biosynthetic control of the natural abundance of C-13 at specific positions within fatty acids in *Escherichia coli*—Evidence regarding the coupling of fatty acid and phospholipid synthesis, *J. Biol. Chem.*, *255*(23), 1435–1441.

Newman, B. D., et al. (2015), Microtopographic and depth controls on active layer chemistry in Arctic polygonal ground, *Geophys. Res. Lett.*, *42*, 1808–1817, doi:10.1002/2014GL062804.

Oremland, R. S. (1988), Biology of anaerobic microorganisms, in *Biogeochemistry of Methanogenic Bacteria*, edited by Z. AJB, pp. 641–705, John Wiley, New York.

Owens, E. H., and J. R. Harper (1977), Frost-table and thaw depths in the littoral zone near Pearl Bay, Alaska, *Arctic*, *30*, 155–68.

Popp, T. J., J. P. Chanton, G. J. Whiting, and N. Grant (1999), Methane stable isotope distribution at a carex dominated fen in North Central Alberta, *Global Biogeochem. Cycles*, *13*(4), 1063–1077.

Preuss, I., C. Knoblauch, J. Gebert, and E. M. Pfeiffer (2013), Improved quantification of microbial CH_4 oxidation efficiency in arctic wetland soils using carbon isotope fractionation, *Biogeosciences*, *10*(4), 2539–2552.

Reeburgh, W. S., A. I. Hirsch, F. J. Sansone, B. N. Popp, and T. M. Rust (1997), Carbon kinetic isotope effect accompanying microbial oxidation of methane in boreal forest soils, *Geochim. Cosmochim. Acta*, *61*(22), 4761–4767.

Rhew, R. C., Y. A. Teh, and T. Abel (2007), Methyl halide and methane fluxes in the northern Alaskan coastal tundra, *J. Geophys. Res.*, *112*, G02009, doi:10.1029/2006JG000314.

Rooney-Varga, J. N., M. W. Giewat, K. N. Duddleston, J. P. Chanton, and M. E. Hines (2007), Links between archaeal community structure, vegetation type and methanogenic pathway in Alaskan peatlands, *Fems Microbiol. Ecol.*, *60*(2), 240–251.

Rovansek, R. J., L. D. Hinzman, and D. L. Kane (1996), Hydrology of a tundra wetland complex on the Alaskan Arctic Coastal Plain, USA, *Arct. Alp. Res.*, *28*(3), 311–317.

Roy Chowdhury, T., E. M. Herndon, T. J. Phelps, D. A. Elias, B. Gu, L. Liang, S. D. Wullschleger, and D. E. Graham (2015), Stoichiometry and temperature sensitivity of methanogenesis and CO_2 production from saturated polygonal tundra in Barrow, Alaska, *Global Change Biol.*, *21*, 722–737, doi:10.1111/gcb.12762.

Rubino, M., et al. (2013), A revised 1000 year atmospheric delta C-13-CO_2 record from Law Dome and South Pole, Antarctica, *J. Geophys. Res. Atmos.*, *118*, 8482–8499, doi:10.1002/jgrd.50668.

Schütz, H., P. Schroder, and H. Rennenberg (1991), Role of plants in regulating the methane flux to the atmosphere, edited by H. Mooney, E. Holland, and T. Sharkey, Trace Gas Emissions from Plants, Academic Press, pp. 29–64.

Schuur, E. A. G., et al. (2008), Vulnerability of permafrost carbon to climate change: Implications for the global carbon cycle, *BioScience*, *58*(8), 701–714.

Seeberg-Elverfeldt, J., M. Schluter, T. Feseker, and M. Kolling (2005), Rhizon sampling of porewaters near the sediment-water interface of aquatic systems, *Limnol. Oceanogr.: Methods*, *3*, 361–371.

Sloan, V. L., J. D. Brooks, S. J. Wood, J. A. Liebig, J. Siegrist, C. M. Iversen, and R. J. Norby (2014), Plant community composition and vegetation height, Barrow, Alaska, ver. 1. Next Generation Ecosystem Experiments Arctic Data Collection, Carbon Dioxide Information Analysis Center, Oak Ridge National Laboratory, Oak Ridge, Tenn. Data set accessed at doi:10.5440/1129476.

Teh, Y. A., E. A. Dubinsky, W. L. Silver, and C. M. Carlson (2008), Suppression of methanogenesis by dissimilatory Fe(III)-reducing bacteria in tropical rain forest soils: Implications for ecosystem methane flux, *Global Change Biol.*, *14*(2), 413–422.

Templeton, A. S., K. H. Chu, L. Alvarez-Cohen, and M. E. Conrad (2006), Variable carbon isotope fractionation expressed by aerobic CH_4-oxidizing bacteria, *Geochim. Cosmochim. Acta*, *70*(7), 1739–1752.

Torn, M. S., and F. S. Chapin (1993), Environmental and biotic controls over methane flux from Arctic tundra, *Chemosphere*, *26*(1–4), 357–368.

Throckmorton, H. T., J. M. Heikoop, B. D. Newman, and C. J. Wilson (2015), Inorganic carbon isotopes and chemical characterization of watershed drainages, Barrow Alaska 2013, Next Generation Ecosystem Experiments Arctic Data Collection, Carbon Dioxide Information Analysis Center, Oak Ridge Natl. Lab., Oak Ridge, Tenn., doi:10.5440/1221564.

Verville, J. H., S. E. Hobbie, F. S. Chapin, and D. U. Hooper (1998), Response of tundra CH_4 and CO_2 flux to manipulation of temperature and vegetation, *Biogeochemistry*, *41*(3), 215–235.

Villarreal, S., R. D. Hollister, D. R. Johnson, M. J. Lara, P. J. Webber, and C. E. Tweedie (2012), Tundra vegetation change near Barrow, Alaska (1972–2010), *Environ. Res. Lett.*, *7*(1), doi:10.1088/1748-9326/7/1/015508.

von Fischer, J. C., and L. O. Hedin (2007), Controls on soil methane fluxes: Tests of biophysical mechanisms using stable isotope tracers, *Global Biogeochem. Cycles*, *21*, GB2007, doi:10.1029/2006GB002687.

von Fischer, J. C., R. C. Rhew, G. M. Ames, B. K. Fosdick, and P. E. von Fischer (2010), Vegetation height and other controls of spatial variability in methane emissions from the Arctic coastal tundra at Barrow, Alaska, *J. Geophys. Res.*, *115*, G00I03, doi:10.1029/2009JG001283.

Wainwright, H. M., B. Dafflon, L. J. Smith, M. S. Hahn, J. B. Curtis, Y. X. Wu, C. Ulrich, J. E. Peterson, M. S. Torn, and S. S. Hubbard (2015), Identifying multiscale zonation and assessing the relative importance of polygon geomorphology on carbon fluxes in an Arctic tundra ecosystem, *J. Geophys. Res. Biogeosci.*, *120*, 788–808, doi:10.1002/2014JG002799.

Whalen, S. C., W. S. Reeburgh, and K. A. Sandbeck (1990), Rapid methane oxidation in a landfill cover soil, *Appl. Environ. Microbiol.*, *56*(11), 3405–3411.

Whiticar, M. J. (1999), Carbon and hydrogen isotope systematics of bacterial formation and oxidation of methane, *Chem. Geol.*, *161*(1–3), 291–314.

Whiticar, M. J., E. Faber, and M. Schoell (1986), Biogenic methane formation in marine and fresh-water environments—CO_2 reduction vs acetate fermentation isotope evidence, *Geochim. Cosmochim. Acta*, *50*(5), 693–709.

Woo, M. K., D. L. Kane, S. K. Carey, and D. Q. Yang (2008), Progress in permafrost hydrology in the new millennium, *Permafrost Periglac. Process.*, *19*(2), 237–254.

Zhang, Z., D. L. Kane, and L. D. Hinzman (2000), Development and application of a spatially-distributed Arctic hydrological and thermal process model (ARHYTHM), *Hydrol. Process.*, *14*(6), 1017–1044.

Zona, D., W. C. Oechel, K. M. Peterson, R. J. Clements, K. T. PAW U, and S. L. Ustin (2010), Characterization of the carbon fluxes of a vegetated drained lake basin chronosequence on the Alaskan Arctic Coastal Plain, *Global Change Biol.*, *16*(6), 1870–1882, doi:10.1111/j.1365-2486.2009.02107.x.

Zona, D., D. A. Lipson, R. C. Zulueta, S. F. Oberbauer, and W. C. Oechel (2011), Microtopographic controls on ecosystem functioning in the Arctic Coastal Plain, *J. Geophys. Res.*, *116*, G00I08, doi:10.1029/2009JG001241.